Radiation responses of 2D and 3D glioblastoma cells: a novel, 3D-specific radioprotective role of VEGF/Akt signaling through functional activation of NHEJ

1. Natividad Gomez-Roman
2. Ming Y Chong
3. Sandeep K Chahal
4. Seamus P Caragher
5. Mark R Jackson
6. Katrina H Stevenson
7. Sidhartha A Dongre
8. Anthony J Chalmers

Author affiliations: [1—8] Wolfson Wohl Translational Cancer Research Centre, Institute of Cancer Sciences, University of Glasgow

Running Title: VEGF/Akt radioprotects 3D glioblastoma cells through NHEJ

Keywords: Glioblastoma, three-dimensional, VEGF, ionising radiation, DNA-PKcs

Corresponding author: Natividad Gomez-Roman, Wolfson Wohl Translational Cancer Research Centre, Institute of Cancer Sciences, University of Glasgow, Garscube Estate, Glasgow G61 1BD. Email: n.gomez-roman@beatson.gla.ac.uk; Tel. 00 44 141 3303984

Potential conflicts of interest: The authors declare no potential conflicts of interest.

Abstract

Glioblastoma is resistant to conventional treatments and has dismal prognosis. Despite promising in vitro data, molecular targeted agents have failed to improve outcomes in patients, indicating that conventional two-dimensional (2D) in vitro models of GBM do not recapitulate the clinical scenario. Responses of primary glioblastoma stem-like cells (GSC) to radiation in combination with EGFR, VEGF and Akt inhibition were investigated in conventional 2D cultures and a 3-dimensional (3D) *in vitro* model of GBM that recapitulates key GBM clinical features. VEGF deprivation had no effect on radiation responses of 2D GSC but enhanced radiosensitivity of GSC cultures in 3D. The opposite effects were observed for EGFR inhibition. Detailed analysis of VEGF and EGF signalling demonstrated a radioprotective role of Akt that correlates with VEGF in 3D and with EGFR in 2D. In all cases, positive correlations were observed between increased radiosensitivity, markers of unrepaired DNA damage and persistent phospho-DNA-PK nuclear foci. Conversely, increased numbers of Rad51 foci were observed in radioresistant populations, indicating a novel role for VEGF/Akt signalling in influencing radiosensitivity by regulating the balance between non-homologous end-joining and homologous recombination mediated DNA repair. Differential activation of tyrosine kinase receptors in 2D and 3D models of GBM explains the well documented discrepancy between pre-clinical and clinical effects of EGFR inhibitors. Data obtained from our 3D model identify novel determinants and mechanisms of DNA repair and radiosensitivity in GBM, and confirm Akt as a promising therapeutic target in this cancer of unmet need.

Introduction

Glioblastoma (GBM) is the most common and aggressive malignant primary brain tumour [1]. Tumours exhibit inherent resistance to radiation and chemotherapy with 5 year survival rates of ~4% [2,3]. Radiation resistance of GBM has been attributed to a subpopulation of cancer cells termed 'GBM stem-like cells' (GSC) which express stem cell markers, can differentiate into different lineages and have potent tumorigenic capacity [4-10]. To improve clinical outcomes, the molecular mechanisms underlying radio- and chemoresistance of GSC need to be elucidated. However, novel targeted agents that have shown pre-clinical activity in conventional GBM cell culture systems have consistently failed to achieve clinical efficacy.

One explanation for the discrepancy between preclinical and clinical data is the widespread use of preclinical models that fail to recapitulate the *in vivo* scenario. Lack of clinical efficacy of new agents might be explained by misleading preclinical data generated in established cancer cell lines cultured in simplified two-dimensional (2D) *in vitro* systems, in which cells undergo profound phenotypical changes and exhibit markedly different responses to cytotoxic treatments [11-14]. In the context of radiation therapy, 3D culture of lung and head & neck cancer cells embedded in laminin-rich extracellular matrix (lrECM) has been shown to promote radiation resistance compared to 2D culture [15,16]. Likewise, colorectal cancer cell lines cultured under similar 3D conditions exhibited changes in cellular morphology, phenotype and gene expression and were resistant to epidermal growth factor receptor (EGFR) inhibition compared to cells cultured in 2D conditions [17]. We have recently demonstrated lack of response to the EGFR tyrosine kinase inhibitor erlotinib either alone or in combination with radiation in a novel 3D model of GBM consisting of patient-derived GSC grown on 3D-Alvetex® scaffolds (3D), whereas

radiosensitisation was clearly observed in 2D GSC [14]. These findings recapitulate those of clinical trials in GBM in which treatments targeting EGFR either through the tyrosine kinase inhibitors erlotinib or gefitinib, or the anti-EGFR antibody cetuximab showed very low response rates and in some cases yielded inferior outcomes and/or worse toxicity than standard of care [18-30], despite clear evidence of preclinical activity against established cell lines grown as 2D cultures. Taken together, these observations provide some insight into why results derived in conventional 2D cell culture systems are so often poorly predictive of clinical efficacy.

Anti-vascular endothelial growth factor (VEGF) therapy has also been evaluated in GBM, yielding marginally better clinical outcomes. Hypoxia is a cardinal feature of GBM, and is associated with high levels of vascular endothelial growth factor (VEGF) [31,32]. Increased VEGF expression correlates with poor prognosis and treatment resistance in GBM [33,34] and addition of anti-VEGF therapy (e.g. bevacizumab) to standard radio-chemotherapy increases progression-free survival but not overall survival [35,36]. While anti-VEGF therapy was developed primarily to target the tumour vasculature, GBM cells also express VEGF receptor 2 (VEGFR2) and are thus potential targets [14,37], unlike normal brain in which VEGFR2 expression is undetectable. Previous studies have reported protective effects of VEGF on GBM cells treated with paclitaxel or radiation [38] that were mediated via VEGFR2. VEGFR2 inhibition has also been shown to reduce GSC viability and survival *in vivo* [37]. We have recently added to this literature by showing that the anti-VEGF monoclonal antibody bevacizumab increases radiosensitivity in a customised 3D GSC system but has no effect in conventional 2D cultures [14].

To interrogate these novel observations further, and elucidate the underlying mechanisms, we used our customised, validated 3D GBM model to investigate

whether the radiosensitising effects of VEGF inhibition are mediated via the DNA damage response (DDR). In this model, downregulation of VEGF signalling consistently induced a radiosensitive phenotype that was associated with aberrant NHEJ, inhibition of HR and accumulation of unrepaired DNA damage. We went on to show that the radiosensitising effects of VEGF depletion in 3D and EGFR inhibition in 2D cultures are mediated by the downstream signalling protein Akt. In addition, our data indicate that radiation induced changes in the sub-cellular localisation of EGFR are regulated by VEGF signalling.

Materials and Methods

Cell Culture and Radiation Treatment

E2, R10 and G7 GBM cell lines were obtained from Colin Watts laboratory, derived from anonymised patient resection specimens as previously described [39]. Cell lines were routinely cultured on Matigel™-coated plates (0.2347mg/ml in Adv/DMEM) in cancer stem cell optimised serum-free medium comprising Advanced/DMEM/F12 medium (GIBCO) Supplemented with 1% B27 (Invitrogen), 0.5% N2 (Invitrogen), 4μg/ml heparin, 10ng/ml fibroblast growth factor 2 (bFGF,Sigma), 20ng/ml epidermal growth factor (EGF, Sigma) and 1% L-glutamine and used for experiments between passage 3 and 8. For Alvetex® 3D cultures (3D-A), Alvetex® scaffolds were coated with diluted Matrigel™ as for 2D conditions. Cells were irradiated using an RS225 XStrahl machine, at 195 kV, 15 mA with a 0.5 copper filter, at a dose of 2.47 Gy/min. Cells were routinely tested every three months for mycoplasma always tested negative for mycoplasma contamination. Authentication of cells with Illumina Infinium Methylation Analysis in 2017.

Mouse experiments

Female CD1 nude mice were anaesthetised using isofluorane and a 1cm incision was made through the skin along the length of the skull. A hole was drilled through the skull 3 mm posterior to the bregma, and 2 mm lateral to the midline. Inoculation of tumour cells was performed using a digital stereotaxic frame (Harvard Apparatus). A programmable injector pump (Harvard Apparatus) was used to inject $1x10^5$ GSC in 5μl PBS 3mm deep into the brain at a rate of 2μl/min.

Partial brain irradiation encompassing xenograft tumours was performed using the XStrahl small animal radiation research platform (SARRP). Mice were irradiated with 220 kV (peak) X-ray beams at a dose of 4.8 Gy/min using a 5x5 mm collimator with parallel opposed beams under the guidance of cone-beam CT.

Ethical approval

Animal experiments were in compliance with all regulatory guidelines, as described in the Animals Act 1986 Scientific Procedures on living animals regulated by the Home Office in the United Kingdom.

Clonogenic assays

Cells were seeded on Matrigel™-coated plates / 3D-Alvetex scaffolds (0.2374mg/ml). Seeding densities were as follows; 0-2 Gy – 300 cells / well (c/w); 3 Gy, 500 c/w; 4 Gy, 800 c/w; 5-9 Gy, 1000 c/w. 18 hrs after seeding, cells were either sham irradiated or irradiated at indicated doses and incubated for 2.5 (2D) or 3 weeks (3D) prior to fixation with methanol and crystal violet staining for 2D conditions, or thiazolyl blue tetrazolium bromide (MTT) staining followed by 2% paraformaldehyde (PFA)/PBS for 3D conditions. Visible colonies were manually counted. Dose modifying factor (DMF) at 0.37% and 0.1% survival were calculated for each

147 treatment combination as well as sensitizing enhancement ratio (SER) to whole
148 curve as in [40].

149 For knockdown experiments, cells were transfected with respective siRNAs (Table
150 S1A) using Lipofectamine RNAiMax reagent according to manufacturer's instructions.
151 After 48 h incubation, cells were detached with Accutase, counted and seeded in 3D-
152 Alvetex Scaffolds at corresponding densities. 18 h after seeding, cells were
153 irradiated at different doses (0-5 Gy) and incubated for 3 weeks. Clonogenic survival
154 graphs represent mean plus SD of 3 independent experiments. Curves are fitted to a
155 linear quadratic model and are normalised to respective 0 Gy control.

156 For 96-well clonogenics, cells were seeded (G7 -100 c/w, G1 – 200 c/w), incubated
157 for 16 h, treated with respective compounds, incubated for 2 h, irradiated at 0 or 3
158 Gy, and incubated for 13 days prior to colony staining and fixing.

159 Data was analysed using the median effect dose
160 (https://pdfs.semanticscholar.org/6e6f/5f9d670c203ade39e49dec5920fc759d5b67.p
161 df) and Bonferroni's statistical test.

162 **Immunofluorescence**

163 Cells (5 x 10^4 c/w) were seeded on Matrigel-coated coverslips or Matrigel-coated
164 Alvetex® Scaffolds were exposed to erlotinib (1 μM), MK-2206 with a chemical name
165 of 8-[4-(1-aminocyclobutyl)phenyl]-9-phenyl-1,2,4-triazolo[3,4-*f*][1,6]naphthyridin-
166 3(2*H*)-one hydrochloride [1:1] [41](1 μM) or vehicle and treated with 5 Gy or sham
167 irradiated. Cultures were fixed in 2% PFA/PBS at the indicated time points,
168 permeabilised with 1% Triton/PBS, blocked with 2% BSA/TBS/0.5% Tween-20 and
169 incubated with the respective primary antibodies, followed by appropriate secondary

Alexa Fluor 568 or 488 secondary antibodies (Invitrogen, 1:400). Nuclei were counterstained with DAPI in mounting medium (VectaShield). For γH2AX, pDNA-PK and Rad51 foci quantification Z-stacks were obtained at 63× magnification on a Zeiss 780 confocal microscope. The number of nuclei analysed for each data point ranged from 30 to 50 nuclei. Foci per nucleus were counted manually.

For mitotic catastrophe, micronuclei and mitotic analysis, 3D cells were grown in Alvetex scaffolds for 4 days and then mock-irradiated or irradiated (5 Gy). Cells were fixed with 4% paraformaldehyde 24 h after radiation treatment. Scaffolds were immunostained for the mitotic marker phospho-S10 histone H3 (green) to visualise mitotic and mitotic catastrophe cells. DAPI was used to stain for DNA (blue). An average of 350 nuclei / condition / experiment were identified randomly and scored. Percentages of cells displaying micronuclei, mitosis or mitotic catastrophe per nucleus were calculated. Mean ± SEM of 3 independent experiments. *P* values calculated by *t* test.

Protein extraction

2D and 3D cells were exposed to the indicated treatments. For 2D cultures, cells were incubated for 30 minutes in lysis buffer (1% SDS-Tris buffer in the presence of phosphatase and protease inhibitors), scraped from plastic and clarified using Qiagen columns. For 3D cultures, scaffolds were incubated in lysis buffer for 25 min on ice, transferred to a rotating platform at 100 rpm and incubated for 5 minutes. Recovered lysate was clarified using Qiagen columns as for 2D lysates. Lysates were prepared using LDS sample buffer (Life Technologies) in the presence of 1 μM DTT, blotted onto nitrocellulose membrane and probed with specific antibodies (Table S1B).

Results

Differential radiosensitisation by erlotinib and VEGF in 2D and 3D cultures

Elevated VEGF levels are a prominent feature of GBM in general and the GBM stem cell niche in particular, with concentrations reaching above 6000 pg/ml in these tumours [31]. VEGF has been shown to promote self-renewal and survival of GBM cancer stem cells [37] but its impact on their radiation responses is not well characterized. To evaluate whether clinically relevant concentrations of VEGF modulate cellular responses to radiation *in vitro*, effects on clonogenic survival of three different patient-derived GBM cell lines (G7, E2 and R10) were measured under 2D GSC culture conditions and in our novel 3D model [14]. Initially, we performed ELISA assays to measure secretion of VEGF. While all cell lines secreted VEGF in both hypoxic and normoxic conditions, concentrations were significantly lower than have been observed in GBM *in vivo* (Supplementary Fig. S1A). To recapitulate clinically observed levels of VEGF, therefore, media were supplemented with human recombinant VEGF-A (3000 pg/ml). Whereas VEGF supplementation had no effect on clonogenic formation of 2D or 3D GSC in the absence of radiation treatment (Fig. 1A), and did not affect radiosensitivity of 2D cultures, VEGF deprivation was associated with a significant increase in radiation sensitivity of 3D cultures in all three cell lines (Fig. 1B and Supplementary Table S2A). These data are consistent with our previous findings in which bevacizumab caused radiosensitisation in 3D cultures only [14].

EGFR overexpression and/or gene amplification are also common features of GBM. Inhibition of EGFR activity with the specific tyrosine kinase inhibitor erlotinib

decreased phosphorylation of its active site (Y1173) at baseline and in irradiated conditions in both 2D and 3D GSC (Fig. 1C). However, radiosensitisation by erlotinib (1 μM) was only observed in 2D cells (Fig. 1D and Supplementary Table S2B), as previously demonstrated [14]. A likely role for DNA repair in determining selective radiosensitisation of 2D cells by erlotinib was indicated by the observed delay in DSB resolution in 2D cells, as measured by sustained elevation of γH2AX expression in protein extracts (Fig. 1C, compare lane 8 to lane 3). In marked contrast, erlotinib-treated 3D GSC appeared to exhibit faster resolution of γH2AX expression than controls (Fig. 1C, compare lane 11 to lane 16).

To rule out the possibility that lack of radiosensitisation by erlotinib in 3D conditions was due to decreased drug delivery via compound adsorption to the scaffold, we assessed the radiosensitising activity of erlotinib alongside two known radiosensitisers, the PARP inhibitor olaparib and the ATM inhibitor KU-55933[42], across a range of concentrations. Reduced clonogenic efficiency was detected at 3 Gy as expected (Supplementary Fig. S1B). Erlotinib failed to induce radiosensitisation of 3D cultures even at the highest concentration tested (10 μM, Supplementary Fig. S1C), whereas radiosensitisation could be detected with olaparib and KU55933 at nanomolar and micromolar concentrations, respectively (Supplementary Fig. S1D and S1E). These results validate our conclusion that erlotinib has no radiosensitising effect on 3D cells, and render any effect of the scaffold on drug activity very unlikely.

Differential regulation of the downstream signalling molecule Akt in 2D and 3D GSC

In order to characterise the mechanisms by which VEGF and EGFR regulate GSC radiosensitivity we interrogated their key downstream signalling pathway Akt. G7 and E2 cells grown in 2D or 3D conditions were starved of growth factors for 48 hours then induced either with EGF or with VEGF. While EGF treatment induced robust activation of EGFR and phosphorylation of Akt at the early time points in cells grown in 2D conditions, addition of VEGF showed no increment in Akt activation beyond baseline levels (Fig. 2A, left side blots). In contrast, 3D cells showed robust Akt activation upon VEGF stimulation in both G7 and E2 cells (Fig. 2A, right hand blots). EGF stimulation had a modest positive impact on Akt phosphorylation in G7 3D cells at the early time points (Fig. 2A, left panels), remaining at baseline levels in E2 3D cells. Expression of the three Akt isoforms at both mRNA and protein levels was observed in G7 and E2 cell lines (Supplementary Fig. S2A and S2B). Enrichment analysis[43] of RNASeq data derived from G7 and E2 3D cells before and after radiation treatment revealed upregulation of genes involved in the Akt pathway (Supplementary Fig. S2C), supporting a likely role for Akt signalling in mediating radiation responses of 3D GSC.

The divergent effects of EGFR inhibition on radiosensitivity of 2D and 3D GSC cultures prompted us to investigate how the radiation-erlotinib combination affected Akt signalling in these two systems. Erlotinib titration (0.5 μM to 5 μM) showed inhibition of EGFR activity in both 2D and 3D cultures, as demonstrated by decreased phosphorylation of its active site (Y1173) both at baseline and after radiation (Fig. 2B). However, this effect only translated into attenuation of Akt activation in 2D cells, having no effect on Akt activity in the 3D model in the G7 cell line and a reduced effect in E2 cells (Fig. 2B). This is in keeping with our previous observation that EGF plays only a minor role in Akt activation in the 3D system (Fig.

2A). Time course analysis revealed inhibition of radiation induced Akt activity by erlotinib in 2D conditions at early time points (30 min to 3 hrs) (Fig. 2C, left panels), but no effect in 3D conditions (Fig. 2C, right panels). Baseline levels of total Akt were similar in 2D and 3D cells (Fig. 2C). Taken together, our results suggest that Akt activity is differentially regulated in 2D and 3D conditions: by EGF signalling in 2D conditions; and by VEGF signalling in 3D cells.

Akt regulates radiation resistance in 2D and 3D GSC

Having identified a pivotal role for Akt in downstream signalling from VEGF and EGFR, we next investigated its contribution to radiation resistance of 2D and 3D GSC using the specific Akt1/2 inhibitor MK-2206. Treatment of G7 and E2 GSC with MK-2206 (1 μM) consistently inhibited Akt activity in all models, as demonstrated by reduced phosphorylation (Fig. 2D). This effect was accompanied by radiosensitisation in all models (Fig. 3A and 3B, Supplementary Table S2C). In the case of G7 cells, radiosensitisation was not further increased by erlotinib in 2D conditions (Fig. 3A, left graphs) or by VEGF deprivation in 3D conditions (Fig. 3B, left graph). MK-2206 had more pronounced radiosensitising effects on E2 2D cells than erlotinib alone or indeed erlotinib in combination with MK-2206 (Fig. 3A, right graph and Supplementary Table S2C), suggesting that other unidentified upstream signalling factors may be regulating Akt activity in this cell line. In 3D E2 cells, MK-2206 alone and VEGF-deprivation exhibited similar radiosensitising effects whilst the combination of MK-2206 and VEGF-deprivation induced further radiosensitisation (Fig. 3B, right graph and Supplementary Table S2C). These results indicate additive effects of VEGF and Akt inhibition in this cell line. Subsequent experiments confirmed a dose response for the radiosensitizing effect of MK-2206 (Fig. 3C).

To validate that the radiosensitizing effects of MK-2206 were 'on target', the effects of Akt knockdown were evaluated using siRNA targeting of the three Akt isoforms. Downregulation of Akt1 and Akt3 expression at the protein level was detected in E2 cells (Fig. 3D) and was associated with radiosensitisation of E2 3D GSCs (Fig. 3E and Supplementary Table S2D) validating the effects of MK-2206 treatment. Radiosensitising effects were also observed with the Akt inhibitor perifosine (Supplementary Fig. S2D) further confirming the radiosensitising effects of this class of compounds. Overall, these results indicate that radiation sensitivity in GSC is modulated by Akt activity irrespective of the growth conditions.

VEGF deprivation and Akt inhibition are associated with reduced DSB repair and increased mitotic catastrophe in irradiated 3D GSC

Radiation kills cells by damaging DNA and the integrity of the DNA damage response (DDR) is a key determinant of radiosensitivity. More specifically, DNA double strand breaks (DSB) are the most important cytotoxic lesions induced by radiation and are repaired either by the rapid but error-prone non-homologous end-joining (NHEJ) pathway or by homologous recombination (HR) which is accurate but slower and requires the presence of a homologous sister chromatid [44,45]. To investigate the mechanisms underlying the radiosensitising effects of VEGF deprivation and Akt inhibition, quantitative analysis of induction and resolution of radiation induced DSB was performed, using nuclear γH2AX foci as markers of DSB. Delayed resolution of DSB was observed in the VEGF-deprived radiosensitive population compared to the radioresistant VEGF-supplemented 3D populations as shown by increased numbers of unresolved γH2AX foci 24 hours after irradiation (Fig. 4A and B). The possibility that this increase in γH2AX foci was due to a larger proportion of VEGF-deprived cells being in the G2 phase of the cell cycle was

315 excluded by the fact that similar percentages of cells staining positive for the G2
316 phase marker CENPF were detected in both conditions (Supplementary Fig. S3A
317 and S3B, VEGF-enriched 24.44% ±7.62, VEGF-deprived 22.985% ±1.138). No
318 significant differences in γH2AX foci were observed in VEGF-deprived or
319 supplemented cells in the absence of radiation (Fig. 4C). A delay in DSB resolution
320 was also observed in 3D (Fig. 4D) and 2D cells (Fig. 4E) treated with MK-2206 (1
321 μM). More detailed analysis revealed MK-2206 to be associated with increased
322 numbers of γH2AX foci 30 minutes after radiation, suggesting either increased
323 induction of DSB or impairment of early (or 'fast') DSB repair, and at the 24 hour time
324 point (Fig. 4E; representative images in Supplementary Fig. S3C). Unirradiated
325 GSCs treated with MK-2206 exhibited a small but statistically significant increase in
326 median number of foci compared to vehicle at the 24 hour time point, indicating a
327 possible role for Akt in repair of DSB arising from endogenous sources (Fig. 4F).

328 Levels of unresolved DSB at 24 hours correlate with radiation sensitivity both *in vitro*
329 and *in vivo* [44] and have potential to cause cell death by a number of mechanisms
330 including mitotic catastrophe [46,47]. To understand the cell death mechanisms by
331 which inhibition of VEGF or Akt signalling enhances radiosensitivity, quantification of
332 mitotic cells and those undergoing mitotic catastrophe was performed using the
333 specific mitotic marker histone H3 phosphorylated at serine 10 (pS10-H3). Cells
334 undergoing mitotic catastrophe were readily detected as fragmented, pS10-H3
335 positive nuclei (Fig. 4G, red arrows). Whereas numerous cells undergoing mitotic
336 catastrophe were identified in VEGF-deprived 3D cultures 24 hours after irradiation,
337 very few were observed in VEGF-enriched 3D conditions (Fig. 4G and H). An
338 increase in the number of cells exhibiting micronuclei was also observed in the
339 VEGF-deprived populations (Fig. 4H), consistent with the hypothesis that cells

completing mitosis in the presence of unrepaired DNA DSBs generate severe structural chromosomal defects and will eventually succumb. Similar increases in micronuclei were observed in irradiated cells treated with MK-2206 (Supplementary Fig. S3D). Together these results demonstrate that VEGF-deprived 3D cells and Akt inhibited cells are less efficient at repairing radiation induced DNA damage and hence accumulate unresolved DNA DSB that lead eventually to cell death by mechanisms including mitotic catastrophe.

Aberrant NHEJ characterised by persistent DNA-PKcs binding at DSB is associated with the radiosensitising effects of VEGF deprivation or MK-2206 treatment

Cell survival after radiation is determined by both induction of DNA damage and the repair processes that follow. Efficiency and integrity of DSB repair depend on appropriate engagement of either NHEJ or HR, and it has been reported that cancer cells can be susceptible to aberrant DSB repair as a consequence of over-expression or inappropriate activation of NHEJ proteins [48,49]. Approximately 80% of X-ray-induced DSBs are repaired within 2-3 hours by the NHEJ pathway, of which DNA-PKcs is a major catalytic component [50]. Of direct relevance to our experiments, Akt has been shown to activate DNA-PKcs activity in response to radiation [51,52]. To investigate whether delayed resolution of DSBs in the radiosensitised populations was due to diminished NHEJ repair, we quantified the number of phosphorylated DNA-PKcs foci per nucleus in G7 and E2 cells. Unexpectedly, the number of pDNA-PKcs foci 0.5 hours after radiation (5 Gy) was found to be significantly increased in VEGF-deprived, radiosensitive 3D populations compared to the more radioresistant VEGF-enriched 3D cells (Fig. 5A and B). In contrast, VEGF treatment did not affect the number of pDNA-PKcs foci in 2D cultures (Supplementary Fig. S3E).

Quantitative analysis of pDNA-PKcs kinetics over a 24 hour period after radiation treatment showed increased numbers of foci throughout the time course in the radiosensitive VEGF-deprived 3D GSC populations compared to 3D cells grown in the presence of VEGF (Fig. 5A and B). We hypothesized that the presence of large numbers of unresolved pDNA-PKcs foci in VEGF-deprived 3D cells at the 24 hour time point was indicative of ineffective attempts at DSB repair, an interpretation that is supported by the γH2AX data shown in Fig. 3 and the additional observation that these unresolved pDNA-PKcs foci were larger than those observed at earlier time points (Fig 5A, compare 0.5 hrs (-) VEGF image with 24 hrs (-) VEGF image). Consistent with our previous results, we observed a similar increase in the number of pDNA-PKcs foci (red) at the 24 hrs time point in MK-2206 treated 3D cells compared to controls (Fig. 5C). These foci co-localised with γH2AX foci (green), indicating that pDNA-PKcs molecules were accumulating at DSB (Fig. 5C). In order to validate that these DNA-PK foci mediated radiosensitising effects were occurring downstream of VEGF and Akt, clonogenic assays were performed in cells depleted of DNA-PKcs by siRNA targeting. Following siRNA transfection, E2 cells exhibited a significant reduction in DNA-PKcs protein expression and were more radiosensitive than cells transfected with scrambled siRNA (Fig. 5D). Importantly, whereas MK-2206 mediated radiosensitisation persisted in cells expressing scrambled siRNA, no additional radiosensitisation was observed in cells depleted of DNA-PKcs (Fig. 5D and Supplementary Table S2E). These data provide compelling evidence for a novel role for VEGF/Akt signalling in influencing radiosensitivity by interfering with NHEJ through persistent binding of DNA-PKcs to DSB. We postulate that this role has not been identified previously because mechanistic studies have generally been

conducted in 2D *in vitro* cultures in which EGFR signalling is upregulated at the expense of VEGF signalling.

Homologous recombination repair is regulated by VEGF in 3D cultures

It is well established that the NHEJ and HR pathways 'compete' for access to and repair of DSB under certain circumstances, and inhibition of NHEJ has been shown to enhance DSB repair under certain conditions by promoting HR [53]. To test the hypothesis that persistent binding of pDNA-PKcs to DSB inhibits HR repair function, 3D cells in the presence or absence of VEGF were fixed 3 hours after radiation and stained for the key HR protein Rad51. While considerable numbers of Rad51 foci per nucleus were detected in the radioresistant VEGF enriched 3D cells, far fewer foci were visible in the radiosensitive VEGF-deprived 3D cultures at the same time point (Fig. 5E and F). These findings were supported by similar observations when cells were stained for an alternative HR protein BRCA2 (Supplementary Fig. S3F). This effect cannot be explained by a difference in cell cycle distribution as the proportion of CENPF positive G2 cells was not affected by VEGF addition (Supplementary Fig. S3A and S3B). Consistent with the tenet that HR is cell cycle phase specific, functioning only in S and G2 phases during which a sister chromatid DNA template is available for repair, the proportion of nuclei staining positive for Rad51 was not statistically significant to the proportion of CENPF positive cells under the same conditions (Supplementary Fig. S3G). These data indicate that, in this 3D model, VEGF-deprived cells initiate HR at a much lower rate than VEGF-enriched cells and are consistent with a scenario in which VEGF driven activation of Akt promotes rapid and efficient NHEJ, which also permits functional HR. In the absence of VEGF, lack of Akt signalling results in aberrant and prolonged binding of DNA-PKcs to DSB which both delays NHEJ mediated repair and inhibits HR.

414

415 **Activation of VEGFR2 and functional activation of both NHEJ and HR in an**
416 **orthotopic mouse model of GBM**

417 To validate *in vivo* the observations made in the 3D model *in vitro,* we interrogated
418 relevant DDR parameters before and after irradiation in tissue from patient-derived
419 human GBM orthotopic mouse models. We have previously shown phosphorylation
420 and activation of the VEGFR2 receptor in the majority of tumour cells in G7 and E2
421 orthotopic tumours [14] and Supplementary Fig. S4A, confirming that VEGF/VEGFR2
422 signalling is active *in vivo*. Based on our 3D *in vitro* data, we hypothesised that
423 tumour cells in which VEGF signalling pathway is active would exhibit functional
424 NHEJ and that pDNA-PKcs nuclear foci would be detectable at early time points
425 after irradiation *in vivo* and would resolve rapidly. To assess this, CD1 nude mice
426 were injected intracranially with E2 cells and monitored for five months to allow the
427 infiltrative tumour growth pattern characteristic of this model. Following this period,
428 mice underwent partial brain irradiation (10Gy) or mock treatment and were
429 sacrificed at different time points (0, 0.5, 2 and 24 h). Immunofluorescence was
430 performed to evaluate activation of NHEJ by detection of pDNA-PKcs nuclear foci.
431 For this experiment, EGFR was selected as tumour cell marker as it was not
432 expressed in normal mouse brain tissue (Supplementary Fig. S4A). A significant
433 increase in pDNA-PKcs foci was detected 30 minutes after radiation treatment, the
434 vast majority of which had resolved within 2 hours. No foci were detected at the 24
435 hour time point (Fig. 6A). Consistent with these data, Rad51 nuclear foci were
436 detected 4 hours after radiation treatment *in vivo* and had resolved by 24 hours
437 (Supplementary Fig. S4B). These data recapitulate our *in vitro* observations, where
438 3D GSC grown in the presence of VEGF activated Akt and exhibited efficient DSB

repair, with early NHEJ activation followed by HR activation and complete resolution of repair foci by 24 hours.

MK-2206 extends survival in combination with radiation in the U87MGLuc orthotopic xenograft GBM model

We then proceeded to evaluate the efficacy of combining Akt inhibition with radiation *in vivo*. CD1 nude mice were injected intracranially with U87MGLuc cells. Bioluminescence imaging was performed on day 6 confirming tumour engraftment (Supplementary Fig. S4C). At day 13, mice were randomised into 4 cohorts (Fig. 6B), and treated with respective protocols over a two-week period. All treatment regimens were well tolerated, with no significant changes in body weight observed (Fig. 6C). Following this period, mice were monitored daily and sacrificed when symptomatic. While no increase in survival was conferred by the Akt inhibitor MK-2206 alone, the radiation schedule of 6 x 2 Gy (administered on alternate days) was associated with a modest but statistically significant increase in survival ($P < 0.001$), and combined treatment with MK-2206 and radiation conferred additional survival benefit, with a 9-day prolongation in median survival over control or MK-2206 alone ($P < 0.0001$) and a 5-day prolongation in median survival relative to the IR schedule ($P = 0.006$; Fig. 6D and E, Supplementary Table S3).

Erlotinib treatment of VEGF-deprived 3D GSC increases their radiation resistance

While performing clonogenic assays with different treatment combinations, we observed that erlotinib had a marked radioprotective effect on VEGF-deprived 3D cultures in three different patient-derived cell lines (G7, E2, and R10), an effect of the same magnitude as that observed for VEGF treatment in this model (Fig 7A and

Supplementary Fig. S5A). No further radioprotection was detected in the presence of VEGF (Fig. 7A), indicating a correlation between VEGF signalling and EGFR inhibition that has not been documented previously. In contrast, radiosensitisation of 2D cultures by erlotinib was not affected by VEGF (Supplementary Fig. S5B-D). Consistent with these results, the radioresistant erlotinib-treated 3D GSC and the 3D GSC supplemented with VEGF were more efficient at repairing DSBs after radiation treatment, exhibiting lower number of γH2AX foci levels at 24 hrs than the radiosensitive 3D VEGF-deprived cells (Supplementary Fig. S5E). No statistically significant difference was observed in the number of pDNA-PKcs foci and Rad51 foci were observed in the erlotinib-treated VEGF-deprived 3D GSC (Fig. 7B and 7C) and in erlotinib-treated VEGF supplemented 3D GSC (Supplementary Fig. S5F and S5G) as in the VEGF-treated cells at early time points, which were completely resolved at 24 hrs, in contrast to the VEGF-deprived cells without erlotinib which exhibited increased pDNA-PKcs foci at all timepoints and reduced Rad51 foci.

EGFR/DNA-PKcs nuclear colocalisation correlates with aberrant NHEJ and HR in VEGF-deprived radiosensitive populations

Having made the novel and unexpected observation that EGFR inhibition protected 3D GSCs following ionising radiation, we investigated the mechanisms involved. In head and neck carcinomas, EGFR activates repair of radiation induced DSB through phosphorylation of DNA-PKcs [35, 36]. Colocalisation analysis of DNA-PKcs and EGFR was therefore performed in G7 and E2 3D cultures in the radioresistant populations (+VEGF or erlotinib) and the radiosensitive VEGF-deprived cells. Nuclear colocalisation of DNA-PKcs and EGFR was detected in the VEGF-deprived radiosensitive 3D populations at both early (0.5 hours) and late (24 hours) timepoints

after radiation treatment. In contrast, nuclear colocalisation of DNA-PKcs and EGFR could not be observed in the radioresistant G7 3D (Fig. 7D-F) or E2 3D (Supplementary Fig. S5H) populations either before or after irradiation. These findings suggest that, in a clinically relevant 3D model of GBM: (i) VEGF inhibits nuclear localisation of EGFR, (ii) EGFR activation is required for its translocation into the nucleus, and (iii) EGFR/DNA-PKcs complex binding to DSBs requires additional signalling that promotes its disassociation and functional DSB repair.

Discussion

Here we describe a novel role for VEGF/VEGFR2 signalling in the regulation of radiation sensitivity and the DDR using a customised, 3D cell culture system that resembles key histological features of GBM and replicates particular clinical responses to molecular targeted therapies such as EGFR inhibition and temozolomide treatment. Our results provide important insights into the mechanisms by which GSC survive radical radiotherapy. Anti-VEGF therapy (bevacizumab) was developed primarily to target angiogenesis; our 3D model identifies a direct effect of VEGF on tumour cell radiosensitivity that could be exploited to overcome radiation resistance. Credence for the clinical efficacy of targeting VEGF signalling in GBM is provided by recently reported results of a phase II study of the VEGFR, FGFR and PDGFR inhibitor regorafenib in patients with recurrent disease, which showed improved 12 month overall survival (38.9% vs 15.0%) and 6 month progression-free survival (16.9% vs 8.3%) compared with lomustine [54]. A number of potential resistance mechanisms may explain the failure of bevazicumab to extend survival in first line treatment (39), including failure to cross the blood brain barrier and

compensatory roles of other VEGFs (e.g. VEGF-B) or VEGF receptors. More specifically, GSC have been shown to exhibit a VEGF/VEGFR2 autocrine signalling loop associated with a cytosolic VEGFR2 subfraction [37], which might contribute to resistance to VEGF targeting strategies. Our results indicate that tyrosine kinase receptor related mechanisms underlying radioresistance of GBM in general and GSC in particular are worthy of detailed investigation in the future. Further assessment in the 3D model of successful and failed molecular therapies in the clinic will provide meaningful validation of the 3D model for utilisation in preclinical studies of molecular targeted therapies that might predict translational success.

Radioresistance is intimately associated with the DDR, and efficiency and integrity of DSB repair depends on appropriate engagement of NHEJ and/or HR. An increasing body of evidence indicates that cancer cells might be susceptible to aberrant DSB repair as a consequence of over-expression or inappropriate activation of NHEJ proteins including the catalytic subunit DNA-PKcs [51,52]. While EGFR signalling has been shown to modulate DNA DSB repair in general and DNA-PKcs activity in particular [51,52,55,56], to our knowledge there is no published evidence that VEGF signalling influences any aspect of DNA repair. Our previous observations with bevacizumab [14] and the demonstration by Bartek's group that direct inhibition of VEGFR2 reduces GSC viability under conditions of radiation-evoked stress, implied a potential role for VEGF in DNA repair. The data presented here demonstrate for the first time that VEGF can activate DNA repair via Akt and DNA-PKcs functionality, a phenomenon that is only observed in 3D conditions. Furthermore, our studies show for the first time that Akt responds to different cues in 2D and 3D cells. While EGFR regulated Akt activity in 2D cultures, VEGF signalling was required for its activation in the 3D model. Our results are consistent with previous reports that Akt

signalling to DNA-PK promotes functional NHEJ activity and radioprotection, but in previous studies conducted in 2D cultures, the link to VEGF signalling was not appreciated.

Several reports have demonstrated pre-clinical efficacy of the Akt MK-2206 inhibitor in combination with gefitinib) in mouse models of GBM [57,58]. Indeed, clinical trials investigating Akt inhibitors in the treatment of GBM are either underway or in development (e.g. https://clinicaltrials.gov/ct2/show/NCT02430363). Unfortunately a phase I study of MK-2206 in recurrent GBM was terminated prior to enrolment following a re-prioritisation process by the pharmaceutical company. Data from our 3D model strongly support the hypothesis that inhibition of Akt will improve clinical outcomes for GBM and provide further justification for clinical trials in this area. They also indicate that the interplay between EGFR, VEGFR2, Akt and DNA-PKcs and possibly other tyrosine kinase receptors such as PDGF and FGFR is worthy of detailed investigation in the future.

Based on preclinical data, huge amounts of time and money have been devoted to clinical studies targeting EGFR in the treatment of GBM, none of which has been successful. In phase I/II clinical trials, addition of erlotinib to radiotherapy and temozolomide failed to improve outcomes [21,22] and in some cases yielded worse outcomes[26]. The identification in 2D breast and pancreatic cell culture systems of radiation-specific phosphorylation sites of EGFR (Y845 and T654)[59] that induce its translocation to the nucleus and stimulate activation of DNA-PKcs provided a detailed rationale and mechanism of action for combining EGFR inhibitors with radiation. Nuclear translocation of EGFR was observed after radiation treatment in VEGF-deprived, radiosensitive 3D cultures as opposed to VEGF supplemented, radioresistant cell populations suggests important cross-talk between EGFR and

561 VEGFR signalling in the 3D context and warrants further investigation. More
562 generally, discrepancies between the EGFR signalling effects observed in our 3D
563 cultures and those described in previous reports might explain the failure of
564 simplified 2D preclinical models to predict the negative outcomes of clinical trials.

565 In summary, irradiation of GBM stem-like cells in a novel 3D cell culture system has
566 radiosensitisation and revealed previously unreported radioprotective effects of
567 VEGF that are mediate through the NHEJ and HR DNA repair pathways (Fig. 7G).
568 As well as increasing our understanding of the clinical effects and limitations of
569 radiation therapy in the management of patients with GBM, these data support the
570 clinical evaluation of Akt inhibitors in GBM and reinforce the concept that potential
571 treatments for GBM should be evaluated in more representative 3D models before
572 proceeding to *in vivo* and clinical testing.

573

574 **Acknowledgements**

575 Cell lines were kindly donated by Dr Colin Watts, University of Cambridge. This
576 research was funded by a Chief Scientist Office (CSO, grant number ETM/405) to
577 A.Chalmers. We also thank the National Centre for the Replacement, Refinement
578 and Reduction of Animals in Research (NC3Rs) for funding this work (grant
579 reference NC/P001335/1) to A.Chalmers and N. Gomez-Roman.

580

581

582

References

1 Brodbelt, A. *et al.* Glioblastoma in England: 2007-2011. *Eur J Cancer* **51**, 533-542, doi:10.1016/j.ejca.2014.12.014 (2015).

2 Stupp, R. *et al.* Effects of radiotherapy with concomitant and adjuvant temozolomide versus radiotherapy alone on survival in glioblastoma in a randomised phase III study: 5-year analysis of the EORTC-NCIC trial. *Lancet Oncology* **10**, 459-466, doi:Doi 10.1016/S1470-2045(09)70025-7 (2009).

3 Stupp, R. *et al.* Radiotherapy plus concomitant and adjuvant temozolomide for glioblastoma. *New England Journal of Medicine* **352**, 987-996, doi:Doi 10.1056/Nejmoa043330 (2005).

4 Zschenker, O., Streichert, T., Hehlgans, S. & Cordes, N. Genome-wide gene expression analysis in cancer cells reveals 3D growth to affect ECM and processes associated with cell adhesion but not DNA repair. *PLoS One* **7**, e34279, doi:10.1371/journal.pone.0034279 (2012).

5 Luca, A. C. *et al.* Impact of the 3D Microenvironment on Phenotype, Gene Expression, and EGFR Inhibition of Colorectal Cancer Cell Lines. *Plos One* **8** (2013).

6 Pontes Soares, C. *et al.* 2D and 3D-organized cardiac cells shows differences in cellular morphology, adhesion junctions, presence of myofibrils and protein expression. *PloS one* **7**, e38147 (2012).

7 Bao, S. *et al.* Glioma stem cells promote radioresistance by preferential activation of the DNA damage response. *Nature* **444**, 756-760, doi:10.1038/nature05236 (2006).

8 Eramo, A. *et al.* Chemotherapy resistance of glioblastoma stem cells. *Cell Death Differ* **13**, 1238-1241, doi:10.1038/sj.cdd.4401872 (2006).

9 Lathia, J. D. *et al.* Direct in vivo evidence for tumor propagation by glioblastoma cancer stem cells. *PloS one* **6**, e24807 (2011).

10 Singh, S. K., Clarke, I. D., Hide, T. & Dirks, P. B. Cancer stem cells in nervous system tumors. *Oncogene* **23**, 7267-7273 (2004).

11 Bokhari, M., Carnachan, R. J., Cameron, N. R. & Przyborski, S. A. Culture of HepG2 liver cells on three dimensional polystyrene scaffolds enhances cell structure and function during toxicological challenge. *Journal of anatomy* **211**, 567-576 (2007).

12 Benton, G., George, J., Kleinman, H. K. & Arnaoutova, I. P. Advancing Science and Technology Via 3D Culture on Basement Membrane Matrix. *Journal of Cellular Physiology* **221**, 18-25, doi:Doi 10.1002/Jcp.21832 (2009).

13 Eke, I. & Cordes, N. Radiobiology goes 3D: how ECM and cell morphology impact on cell survival after irradiation. *Radiother Oncol* **99**, 271-278, doi:10.1016/j.radonc.2011.06.007 (2011).

14 Gomez-Roman, N., Stevenson, K., Gilmour, L., Hamilton, G. & Chalmers, A. J. A novel 3D human glioblastoma cell culture system for modeling drug and radiation responses. *Neuro Oncol*, doi:10.1093/neuonc/now164 (2016).

15 Storch, K. *et al.* Three-dimensional cell growth confers radioresistance by chromatin density modification. *Cancer research* **70**, 3925-3934 (2010).

16 Hehlgans, S., Lange, I., Eke, I. & Cordes, N. 3D cell cultures of human head and neck squamous cell carcinoma cells are radiosensitized by the focal adhesion kinase inhibitor TAE226. *Radiother Oncol* **92**, 371-378, doi:10.1016/j.radonc.2009.08.001 (2009).

17 Poschau, M. *et al.* EGFR and beta1-integrin targeting differentially affect colorectal carcinoma cell radiosensitivity and invasion. *Radiother Oncol* **116**, 510-516, doi:10.1016/j.radonc.2015.06.005 (2015).

18 van den Bent, M. J. *et al.* Randomized phase II trial of erlotinib versus temozolomide or carmustine in recurrent glioblastoma: EORTC brain tumor group study 26034. *Journal of clinical oncology : official journal of the American Society of Clinical Oncology* **27**, 1268-1274 (2009).

19 Rich, J. N. *et al.* Phase II trial of gefitinib in recurrent glioblastoma. *Journal of clinical oncology : official journal of the American Society of Clinical Oncology* **22**, 133-142 (2004).

20 Brewer, C. J. *et al.* Phase II trial of erlotinib with temozolomide and concurrent radiation therapy in patients with newly-diagnosed glioblastoma multiforme. *Journal of Clinical Oncology* **23**, 130s-130s (2005).
21 Peereboom, D. M. *et al.* Phase II trial of erlotinib with temozolomide and concurrent radiation therapy in patients with newly diagnosed glioblastoma multiforme: Final results. *Neuro-Oncology* **8**, 448-448 (2006).
22 Peereboom, D. M. *et al.* Phase II trial of erlotinib with temozolomide and radiation in patients with newly diagnosed glioblastoma multiforme. *Journal of neuro-oncology* **98**, 93-99 (2010).
23 Vogelbaum, M., Peereboom, D., Stevens, G., Barnett, G. & Brewer, C. Phase II study of erlotinib single agent therapy in recurrent glioblastoma multiforme. *Ejc Supplementaryements* **3**, 135-135 (2005).
24 Vogelbaum, M. A., Peereboom, D., Stevens, G., Barnett, G. & Brewer, C. Phase II trial of the EGFR tyrosine kinase inhibitor erlotinib for single agent therapy of recurrent Glioblastoma Multiforme: Interim results. *Journal of Clinical Oncology* **22**, 121s-121s (2004).
25 Vogelbaum, M. A., Peereboom, D., Stevens, G. H., Barnett, G. H. & Brewer, C. Phase II study of single agent therapy with the EGFR tyrosine kinase inhibitor erlotinib in recurrent Glioblastoma Multiforme. *Annals of Oncology* **15**, 206-207 (2004).
26 Vogelbaum, M. A., Peereboom, D., Stevens, G. H. J., Barnett, G. H. & Brewer, C. Response rate to single agent therapy with the EGFR tyrosine kinase inhibitor erlotinib in recurrent glioblastoma multiforme: Results of a phase II study. *Neuro-Oncology* **6**, 384-384 (2004).
27 Lassman, A. B., Abrey, L. E. & Gilbert, M. R. Response of glioblastomas to EGFR kinase inhibitors. *The New England journal of medicine* **354**, 525-526; author reply 525-526 (2006).
28 Norden, A. D. *et al.* Phase II trials of erlotinib or gefitinib in patients with recurrent meningioma. *J Neurooncol* **96**, 211-217, doi:10.1007/s11060-009-9948-7 (2010).
29 Raizer, J. J. *et al.* A phase II trial of erlotinib in patients with recurrent malignant gliomas and nonprogressive glioblastoma multiforme postradiation therapy. *Neuro Oncol* **12**, 95-103, doi:10.1093/neuonc/nop015 (2010).
30 Raizer, J. J. *et al.* A phase I trial of erlotinib in patients with nonprogressive glioblastoma multiforme postradiation therapy, and recurrent malignant gliomas and meningiomas. *Neuro Oncol* **12**, 87-94, doi:10.1093/neuonc/nop017 (2010).
31 Takano, S. *et al.* Concentration of vascular endothelial growth factor in the serum and tumor tissue of brain tumor patients. *Cancer research* **56**, 2185-2190 (1996).
32 Plate, K. H. & Risau, W. Angiogenesis in malignant gliomas. *Glia* **15**, 339-347 (1995).
33 Zhou, Y.-H., Tan, F., Hess, K. R. & Yung, W. K. A. The expression of PAX6, PTEN, vascular endothelial growth factor, and epidermal growth factor receptor in gliomas: relationship to tumor grade and survival. *Clinical cancer research : an official journal of the American Association for Cancer Research* **9**, 3369-3375 (2003).
34 Chaudhry, I. H., O'Donovan, D. G., Brenchley, P. E., Reid, H. & Roberts, I. S. Vascular endothelial growth factor expression correlates with tumour grade and vascularity in gliomas. *Histopathology* **39**, 409-415 (2001).
35 Lai, A. *et al.* Phase II study of bevacizumab plus temozolomide during and after radiation therapy for patients with newly diagnosed glioblastoma multiforme. *Journal of clinical oncology : official journal of the American Society of Clinical Oncology* **29**, 142-148 (2011).
36 Gilbert, M. R. *et al.* A randomized trial of bevacizumab for newly diagnosed glioblastoma. *The New England journal of medicine* **370**, 699-708 (2014).
37 Hamerlik, P. *et al.* Autocrine VEGF-VEGFR2-Neuropilin-1 signaling promotes glioma stem-like cell viability and tumor growth. *J Exp Med* **209**, 507-520, doi:10.1084/jem.20111424 (2012).
38 Yu, Y. *et al.* Knockdown of vascular endothelial cell growth factor expression sensitizes U251 glioma cells to liposomal paclitaxel and radiation treatment in vitro. *Exp Ther Med* **3**, 181-186, doi:10.3892/etm.2011.379 (2012).

39 Fael Al-Mayhani, T. M. *et al.* An efficient method for derivation and propagation of glioblastoma cell lines that conserves the molecular profile of their original tumours. *Journal of neuroscience methods* **176**, 192-199 (2009).
40 Subiel, A., Ashmore, R. & Schettino, G. Standards and Methodologies for Characterizing Radiobiological Impact of High-Z Nanoparticles. *Theranostics* **6**, 1651-1671, doi:10.7150/thno.15019 (2016).
41 Hirai, H. *et al.* MK-2206, an allosteric Akt inhibitor, enhances antitumor efficacy by standard chemotherapeutic agents or molecular targeted drugs in vitro and in vivo. *Mol Cancer Ther* **9**, 1956-1967, doi:10.1158/1535-7163.MCT-09-1012 (2010).
42 Hickson, I. *et al.* Identification and characterization of a novel and specific inhibitor of the ataxia-telangiectasia mutated kinase ATM. *Cancer Res* **64**, 9152-9159, doi:10.1158/0008-5472.CAN-04-2727 (2004).
43 Subramanian, A. *et al.* Gene set enrichment analysis: a knowledge-based approach for interpreting genome-wide expression profiles. *Proc Natl Acad Sci U S A* **102**, 15545-15550, doi:10.1073/pnas.0506580102 (2005).
44 Banath, J. P., Macphail, S. H. & Olive, P. L. Radiation sensitivity, H2AX phosphorylation, and kinetics of repair of DNA strand breaks in irradiated cervical cancer cell lines. *Cancer Res* **64**, 7144-7149, doi:10.1158/0008-5472.CAN-04-1433 (2004).
45 Weterings, E. & Chen, D. J. The endless tale of non-homologous end-joining. *Cell research* **18**, 114-124 (2008).
46 Vitale, I., Galluzzi, L., Castedo, M. & Kroemer, G. Mitotic catastrophe: a mechanism for avoiding genomic instability. *Nat Rev Mol Cell Biol* **12**, 385-392, doi:10.1038/nrm3115 (2011).
47 Mannino, M., Gomez-Roman, N., Hochegger, H. & Chalmers, A. J. Differential sensitivity of Glioma stem cells to Aurora kinase A inhibitors: implications for stem cell mitosis and centrosome dynamics. *Stem cell research* **13**, 135-143 (2014).
48 Neal, J. A. *et al.* Inhibition of homologous recombination by DNA-dependent protein kinase requires kinase activity, is titratable, and is modulated by autophosphorylation. *Molecular and cellular biology* **31**, 1719-1733 (2011).
49 Neal, J. A. *et al.* Unraveling the complexities of DNA-dependent protein kinase autophosphorylation. *Molecular and cellular biology* **34**, 2162-2175 (2014).
50 Kakarougkas, A. & Jeggo, P. A. DNA DSB repair pathway choice: an orchestrated handover mechanism. *Br J Radiol* **87**, 20130685, doi:10.1259/bjr.20130685 (2014).
51 Toulany, M. *et al.* Targeting of AKT1 enhances radiation toxicity of human tumor cells by inhibiting DNA-PKcs-dependent DNA double-strand break repair. *Molecular cancer therapeutics* **7**, 1772-1781 (2008).
52 Toulany, M. *et al.* Akt promotes post-irradiation survival of human tumor cells through initiation, progression, and termination of DNA-PKcs-dependent DNA double-strand break repair. *Molecular cancer research : MCR* **10**, 945-957 (2012).
53 Vartak, S. V. & Raghavan, S. C. Inhibition of nonhomologous end joining to increase the specificity of CRISPR/Cas9 genome editing. *FEBS J* **282**, 4289-4294, doi:10.1111/febs.13416 (2015).
54 Lombardi, G. *et al.* Updated results of REGOMA: A randomized, multicenter, controlled open-label phase II clinical trial evaluating regorafenib in relapsed glioblastoma (GBM) patients (PTS). *Journal of Clinical Oncology* **36**, 2047-2047, doi:10.1200/JCO.2018.36.15_Supplementary.2047 (2018).
55 Friedmann, B. J. *et al.* Interaction of the epidermal growth factor receptor and the DNA-dependent protein kinase pathway following gefitinib treatment. *Molecular cancer therapeutics* **5**, 209-218 (2006).
56 Dittmann, K., Mayer, C., Kehlbach, R. & Rodemann, H. P. Radiation-induced caveolin-1 associated EGFR internalization is linked with nuclear EGFR transport and activation of DNA-PK. *Molecular cancer* **7**, 69 (2008).

57 Cheng, Y. *et al.* MK-2206, a novel allosteric inhibitor of Akt, synergizes with gefitinib against malignant glioma via modulating both autophagy and apoptosis. *Mol Cancer Ther* **11**, 154-164, doi:10.1158/1535-7163.MCT-11-0606 (2012).
58 Narayan, R. S. *et al.* The allosteric AKT inhibitor MK2206 shows a synergistic interaction with chemotherapy and radiotherapy in glioblastoma spheroid cultures. *BMC Cancer* **17**, 204, doi:10.1186/s12885-017-3193-9 (2017).
59 Dittmann, K. *et al.* Nuclear EGFR shuttling induced by ionizing radiation is regulated by phosphorylation at residue Thr654. *FEBS letters* **584**, 3878-3884 (2010).

Figure legends

Figure 1. Radiosensitisation of GSC is determined by growth conditions. **A-B**, Clonogenic efficiency (A) and survival (B) of G7, E2 and R10 GSC grown in 2D and 3D conditions with or without VEGF (3 ng/ml) and irradiated with single doses of X-rays (0-6 Gy; *n=3*). VEGF deprivation significantly increased radiosensitivity of G7, E2 and R10 GSC under 3D conditions (two way ANOVA; p =0.0009, p =0.0056, and p <0.0001, respectively). No significant effect of VEGF was observed in 2D conditions. **C,** Western blot analysis of G7 GSC grown in 2D or 3D conditions and treated with IR (5 Gy) and/or erlotinib (1 μM) at the indicated time points. Actin served as loading control. **D**, Clonogenic survival curves as in (B). Cells were treated with erlotinib (1 μM) for 2 h and then irradiated at different radiation doses (0-6 Gy). All cell lines grown in 2D conditions were significantly radiosensitised by erlotinib (2-way ANOVA analysis: G7 $p < 0.0001$, E2 $p < 0.001$, R10 $p < 0.01$). No radiosensitisation was conferred upon 3D GSC by erlotinib.

Figure 2. Akt regulates EGFR and VEGF radiosensitivity in 2D and 3D GSC, respectively. **A**, G7 and E2 cells grown in 2D or 3D conditions were growth factor-starved for 48 hours followed by addition of EGF (10 ng/ml) or VEGF (3 ng/ml). Cell extracts were prepared at the indicated time points and analysed for total and phospho-EGFR (Y1173) and total and phospho-Akt (S473). S = serum starved; GF =

+EGF and +VEGF for 6 hours. Actin served as loading control. **B,** Protein extracts of G7 (upper blots) and E2 GSCs (lower blots) grown in 2D and 3D conditions in the presence of VEGF and treated for 2 hrs with erlotinib at a range of concentrations (0.5 to 5 μM) followed by radiation treatment (5 Gy) or mock-irradiation. Lysates were prepared 1 hour after irradiation and analysed for total and phosphorylated EGFR and Akt. **C,** E2 GSCs grown in 2D and 3D conditions in the presence of VEGF were treated with vehicle (DMSO) or erlotinib (1 μM) for 2 hrs and ionising radiation (5 Gy) and protein extracts obtained at different time points after irradiation and analysed as in A. **D**, G7 and E2 GSC grown in 2D and 3D conditions in the presence of VEGF were treated with MK-2206 (1 μM) for 2 hours mock-irradiated or treated with ionising radiation (5 Gy). Protein extracts were prepared at different time points. Samples were analysed for total and activated Akt (pAkt at S473) and γH2AX by Western blot. Tubulin served as loading control.

Figure 3. Radiosensitisation of GSC by Akt inhibition. **A**, Clonogenic survival of G7 and E2 GSC grown in 2D conditions and irradiated with single doses of X-rays (0-6 Gy; *n=3*) 1 h after treatment with DMSO, MK-2206 (1 μM) and/or erlotinib (1μM). MK-2206 treatment significantly increased radiosensitivity of G7 and E2 GSC in 2D (two-way ANOVA; G7 2D vs G7 2D + MK-2206 or G7 2D + erlotinib + MK2206 $p<0.0001$; E2 2D vs E2 + MK-2206 or E2 2D + MK-2206 + erlotinib $p<0.0001$, E2 2D vs E2 + erlotinib $p = 0.0006$). **B**, Clonogenic survival of G7 and E2 GSC grown in 3D in conditions as in (A). MK-2206 treatment significantly increased radiosensitivity of G7 and E2 GSC in 3D conditions (two-way ANOVA; G7 3D vs G7 3D + MK-2206 (+) VEGF or G7 3D + MK2206 (-) VEGF $p<0.0001$; E2 3D vs all other conditions $p<0.0001$.) **C**, MK-2206 dose response (0.1 μM to 10 μM) at 0 and 3 Gy in G7 3D GSC. Each curve is normalised to respective vehicle plus radiation dose. **D,** Cell

lysates from E2 cells transfected with siRNA against Akt1, Akt3 or Scramble were analysed for expression of total Akt1, Akt3 after 48 h incubation. Tubulin served as loading control. **E**, Clonogenic assays were performed from E2 cells previously transfected with Scramble or Akt1-3 siRNAs. Akt siRNA cells exhibited increased radiosensitivity compared to Scramble siRNA (two-way ANOVA; siRNA Scramble v all three siRNA Akts $p < 0.0001$).

Figure 4. VEGF deprivation and Akt inhibition reduce DNA double strand break repair following irradiation,of 3D GSC. **A**, Representative immunofluorescent images for γH2AX foci of G7 GSC grown in 3D conditions before (0 h) or after (24 h) ionising radiation (5 Gy) in the presence [(+) VEGF] or absence of VEGF [(-) VEGF]. **B-F**, Quantification of γH2AX foci per nucleus following radiation treatment (5 Gy, B, D and E; or 0 Gy, C and F) in the presence or absence of VEGF (B and C); or DMSO or MK-2206 (D-F). Median ± SD from 3 independent experiments. *P* values calculated by *t* test (* p <0.01; ** p <0.001). **G,** Representative images of 3D cells before and 24 h after irradiation, immunostained for the mitotic marker phospho-S10 histone H3 (green) to visualise mitotic cells. DAPI was used to stain for DNA (blue). Red arrows indicate cells undergoing mitotic catastrophe. **H,** Percentages of cells displaying micronuclei, mitosis or mitotic catastrophe. An average of 350 cells/condition/experiment were identified randomly and scored. Mean ± SEM of 3 independent experiments. *P* values calculated by *t* test.

Figure 5. Functional DNA-PKcs activity correlates with VEGF treatment and Akt activity in the 3D model. **A and C**, Representative immunofluorescent images of E2 GSC grown in 3D conditions and stained for pDNA-PKcs foci (red) at different time points following ionising radiation (5 Gy) in the presence or absence of VEGF (A); or

DMSO or MK-2206 (C). Cells in C were also immunostained for γH2AX foci (green). **B**, Quantification of pDNA-PKcs foci per nucleus following radiation treatment as in **A**. Graphs represent medians from 3 independent experiments. *P* values calculated by *t* test (* $p < 0.01$; ** $p < 0.001$; *** $P < 0.0001$). **D**, Clonogenic assays were performed with E2 cells previously transfected with either scrambled or DNA-PKcs siRNA for 48 hrs. Transfected cells were treated with MK-2206 (1 μM) 16 h after clonogenic seeding, incubated for 2 hrs and irradiated at different doses (0-5 Gy). Cell lysates from E2 cells transfected with siRNA against DNA-PKcs or Scramble were analysed for expression of total DNA-PKcs after 48 hrs incubation. Tubulin served as loading control. **E**, Representative immunofluorescent images of G7 GSC grown in 3D conditions for Rad51 foci at 3 hrs following ionising radiation (5 Gy) in the presence or absence of VEGF. **F**, Quantification of Rad51 foci per nucleus following radiation treatment. Graph represents mean of medians from 3 independent experiments. *p* values calculated by *t* test.

Figure 6. Akt inhibition extends survival of irradiated mice bearing orthotopic glioma xenografts. **A**, Representative immunofluorescent images of paraffin-embedded brains bearing E2 orthotopic tumour cells in mice for pDNA-PKcs S2056 (green). EGFR (red) was used as tumour marker. Mice implanted with E2 cells for 5 months were treated with radiation (10 Gy) and sacrificed at the indicated time points. **B**, Diagram of U87MGLuc2 orthotopic efficacy study, depicting treatment schedules (15 mice/cohort). **C**, Graph depicting mouse body weight monitored from cell implantation until end of treatment. Mice bearing orthotopic xenografts (U87-MGLuc, 13 days after implantation) were randomized into 4 cohorts and treated with the protocols shown in **B**. **D**, Kaplan-Meier survival curves were generated and analysed for log-rank. **E**, Box plot graph of median survival of each treatment group, * $p < 0.05$,

** $p < 0.001$, *** $p < 0.0001$, by one-way ANOVA original FDR method, multiple comparison test.

Figure 7. Erlotinib radioprotects VEGF-deprived 3D GSC by blocking EGFR/DNA-PKcs nuclear co-localisation. **A**, Clonogenic survival of E2 and G7 GSC grown in 3D conditions and irradiated with single doses of X-rays (0-6 Gy; *n=3*) 2 hours after treatment in the presence (+)VEGF or absence (-)VEGF of VEGF and erlotinib (1μM) or vehicle (DMSO). Mean±SD of 3 independent experiments is shown; curves are fitted to a linear quadratic model. Erlotinib significantly radioprotected VEGF-deprived cells (two-way ANOVA; G7 3D (-) VEGF vehicle vs G7 3D (-) VEGF plus erlotinib p<0.0001, E2, p=0.01). No significant effect of erlotinib was observed in the presence of VEGF. **B** and **C**, Quantification of pDNA-PKcs (B) and Rad51 foci (C) per nucleus following radiation treatment. Graph represents mean of medians from 3 independent experiments. *p* values calculated by *t* test (* p <0.01; ** p <0.001).**D,** Representative immunofluorescent images for EGFR (EGFR) and DNA-PKcs (DNA-PKcs) of G7 3D cells following ionising radiation treatment and fixed with paraformaldehyde at the indicated time points (0, 0.5 and 24 hrs). Cells were treated with erlotinib in the absence or presence of VEGF. **E**, Representative immunofluorescent images for the co-localisation of DNA-PKcs and EGFR using Zen Black software by selecting nuclei as regions of interest (red circles) and using the Cut Mask tool following selection and generation of a new image which sets every pixel outside the colocalised pixels to zero and exposing only the pixels where tDNA-PKcs / tEGFR signals are expressed in the same pixel. **F**, Quantification of DNA-PKcs and EGFR colocalisation per nucleus in G7 3D GSC. Approximately 40 nuclei were quantified for each condition. Box and whisker plots represent median number of signal per nucleus, *p* values calculated by Mann Whitney *U* test (*p<0.05;

863 **p<0.005). **G**, Graphic representation of glioblastoma responses to EGF and VEGF
864 signalling in 2D and 3D conditions, respectively, with Akt acting as the main switch
865 between NHEJ and HR resulting in radiation sensitization (aberrant NHEJ) or
866 protection (HR activation).

867

868

869

870

871

872

873

Figure 1

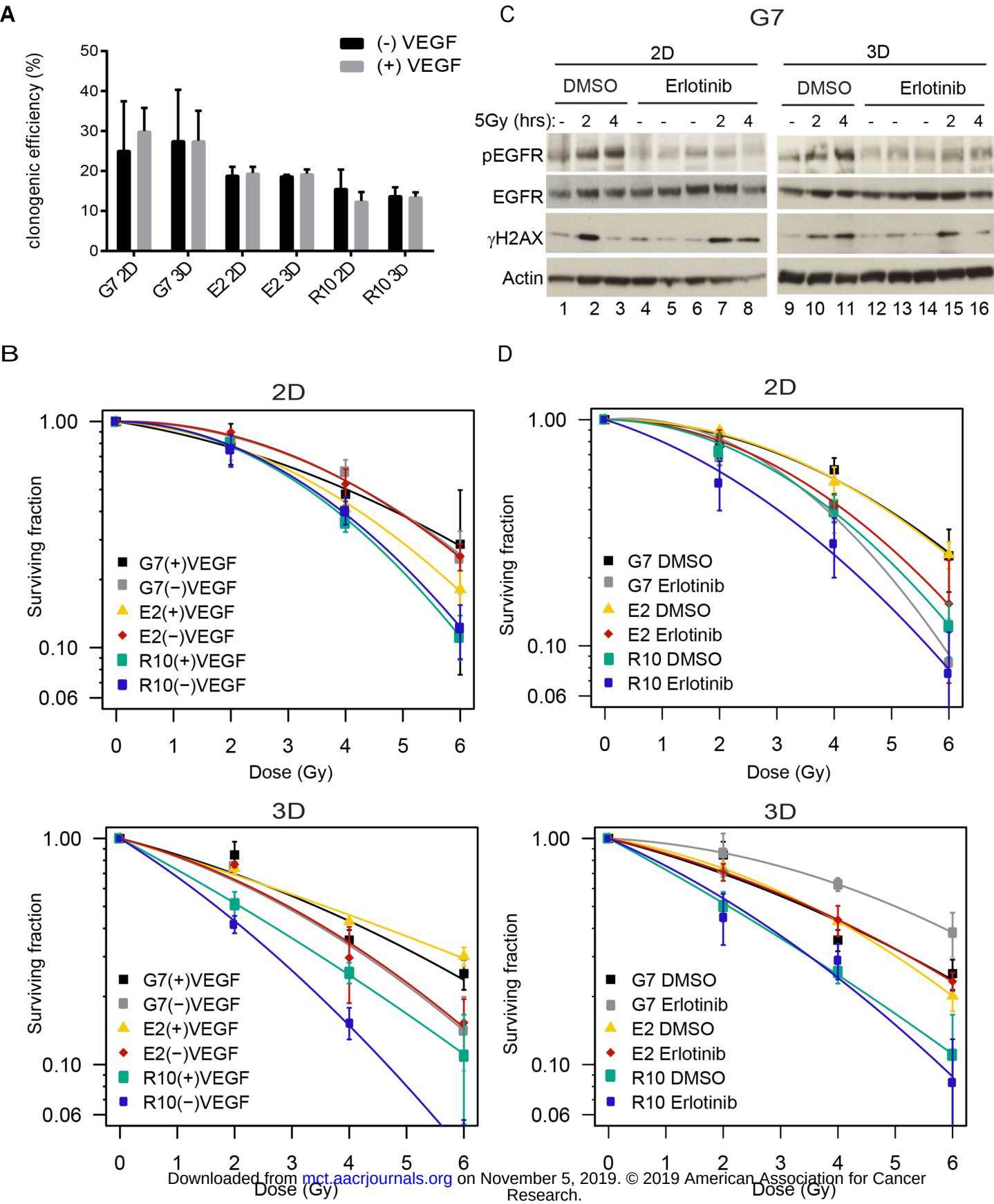

Figure 2

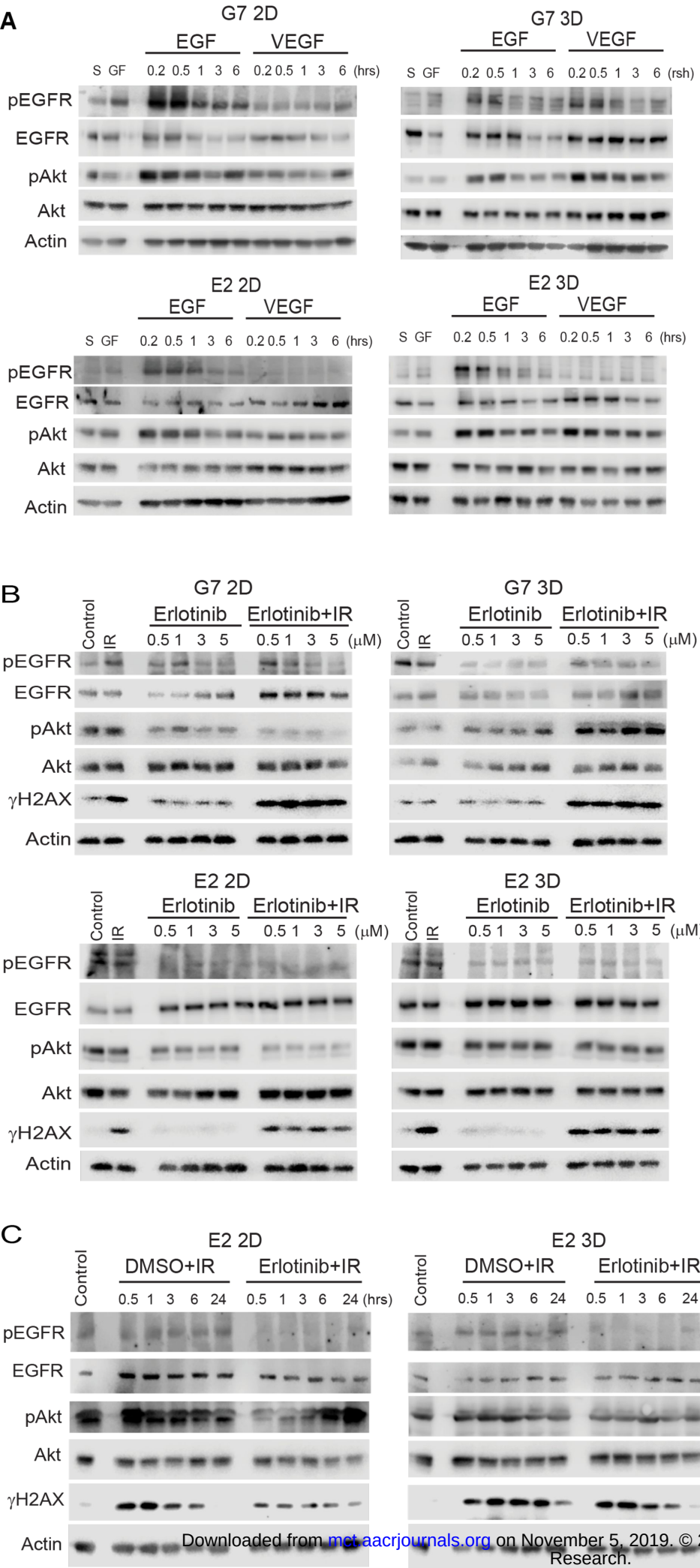

Figure 3

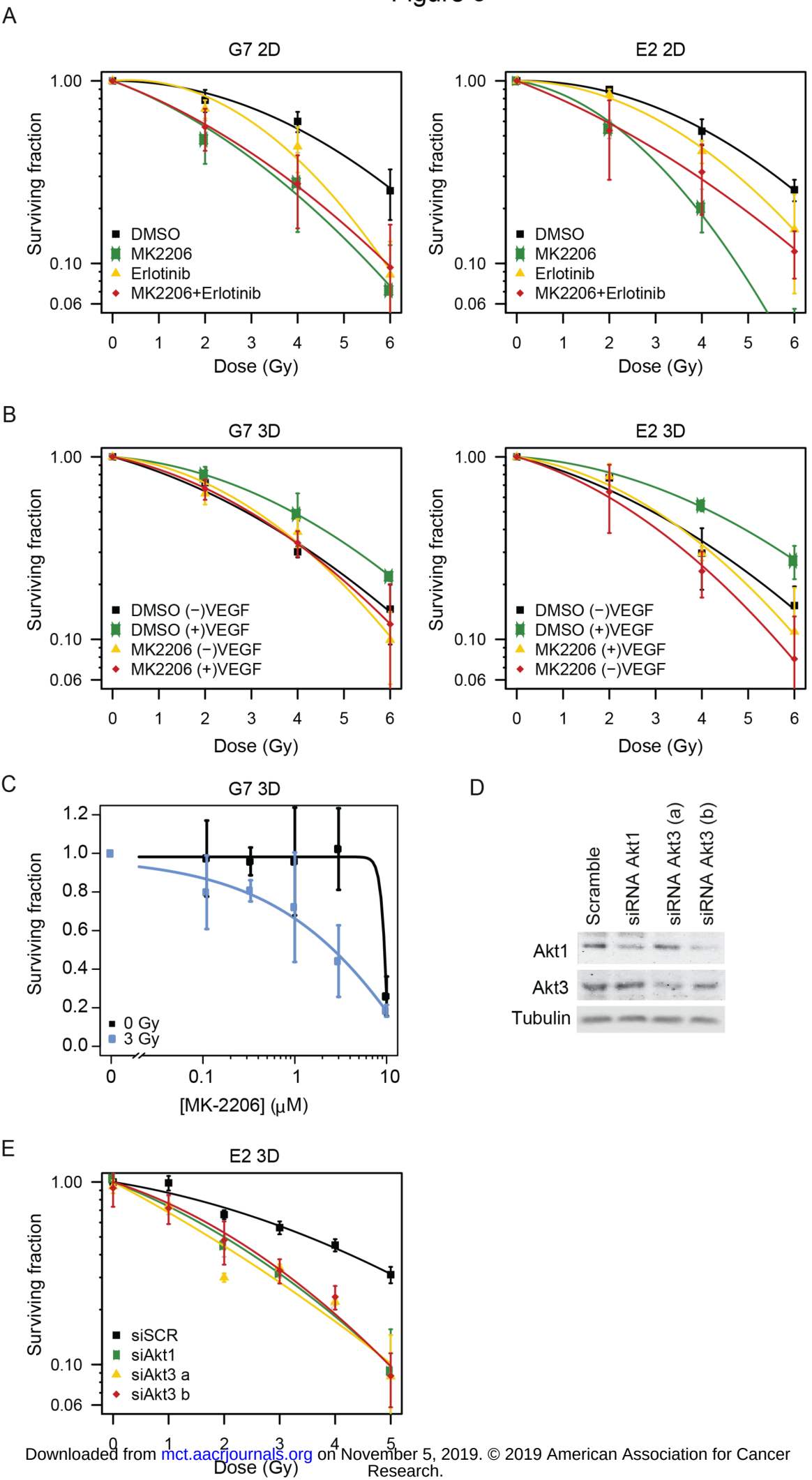

Figure 4

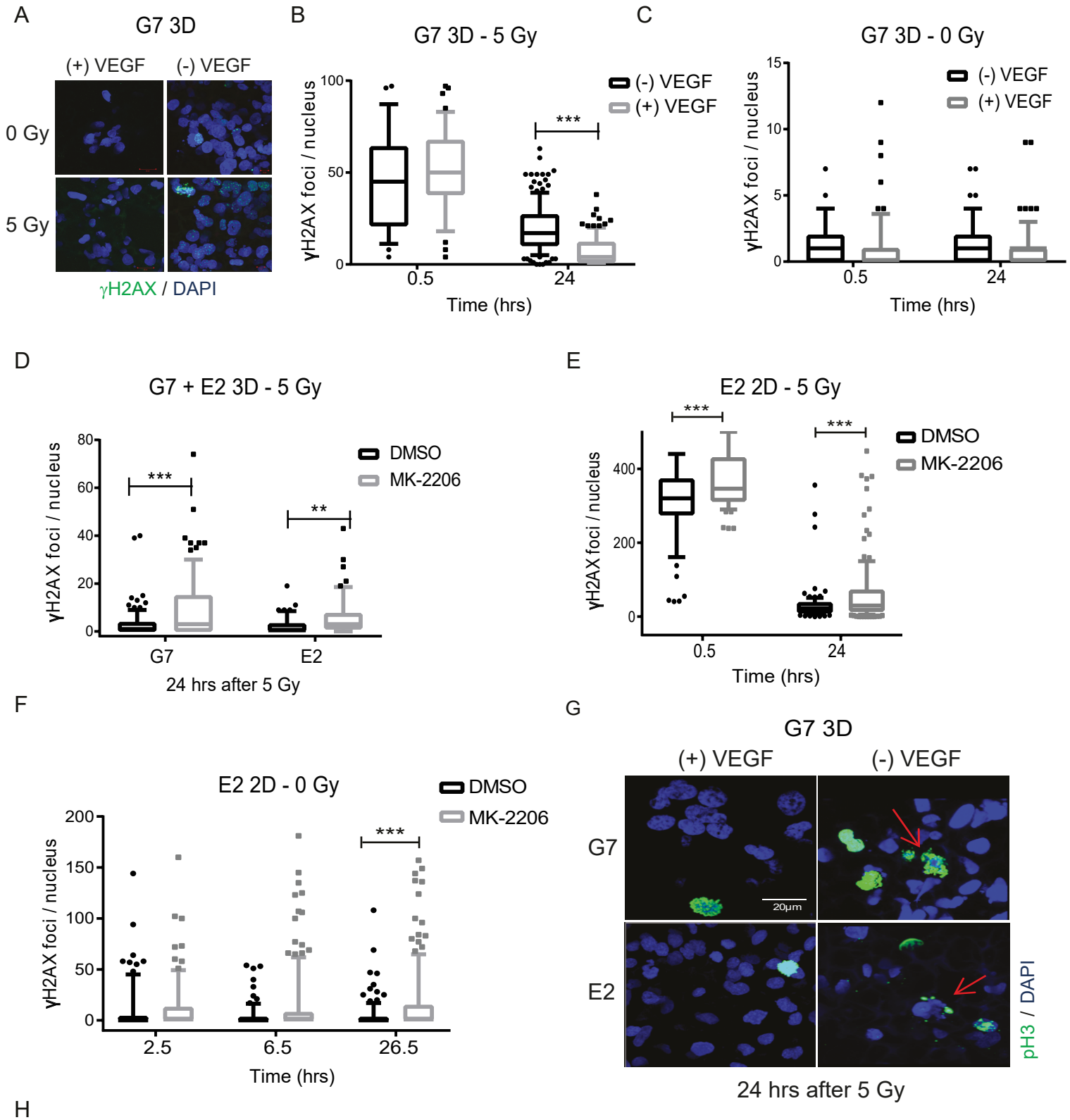

Figure 5

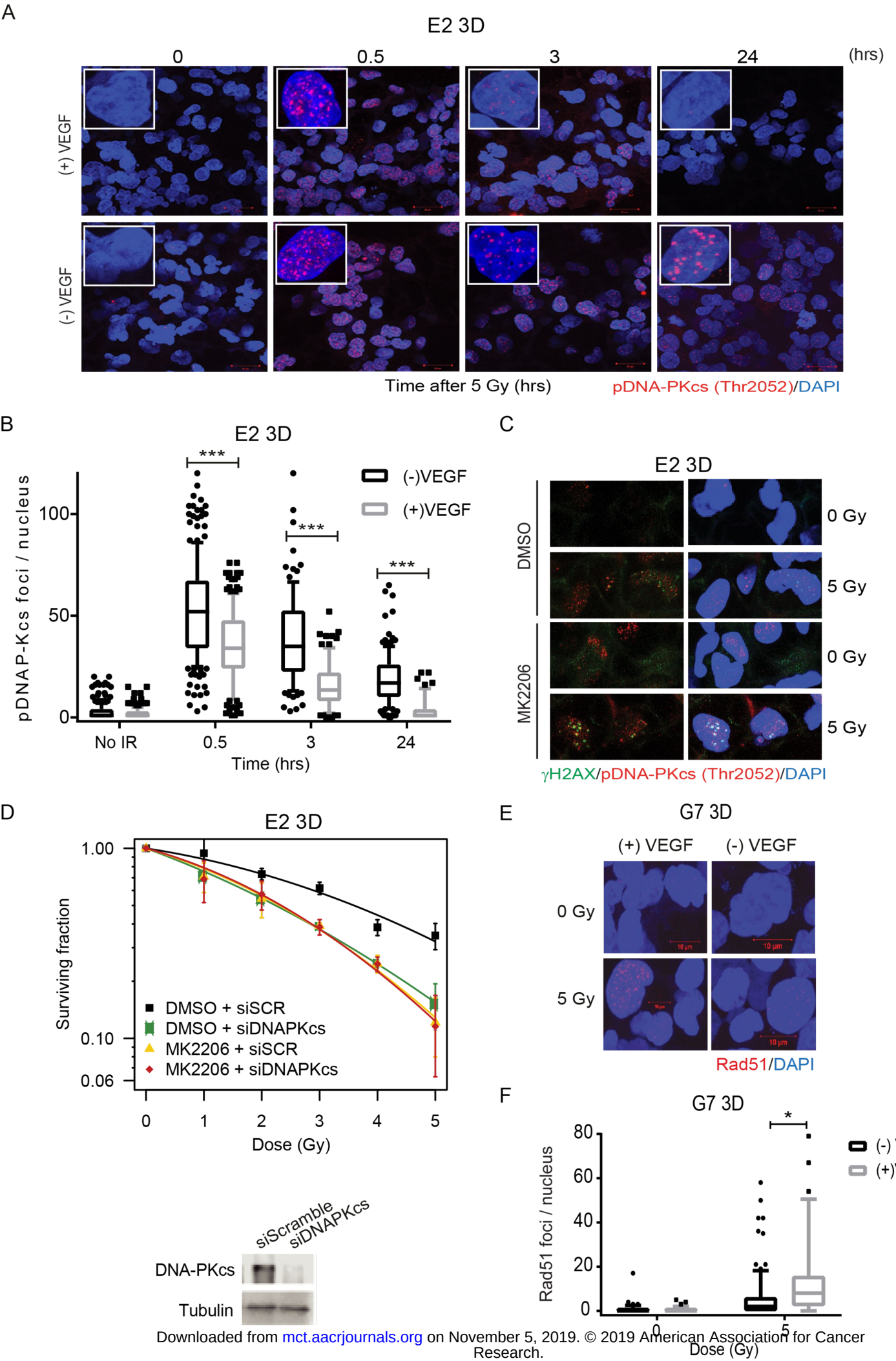

Figure 6

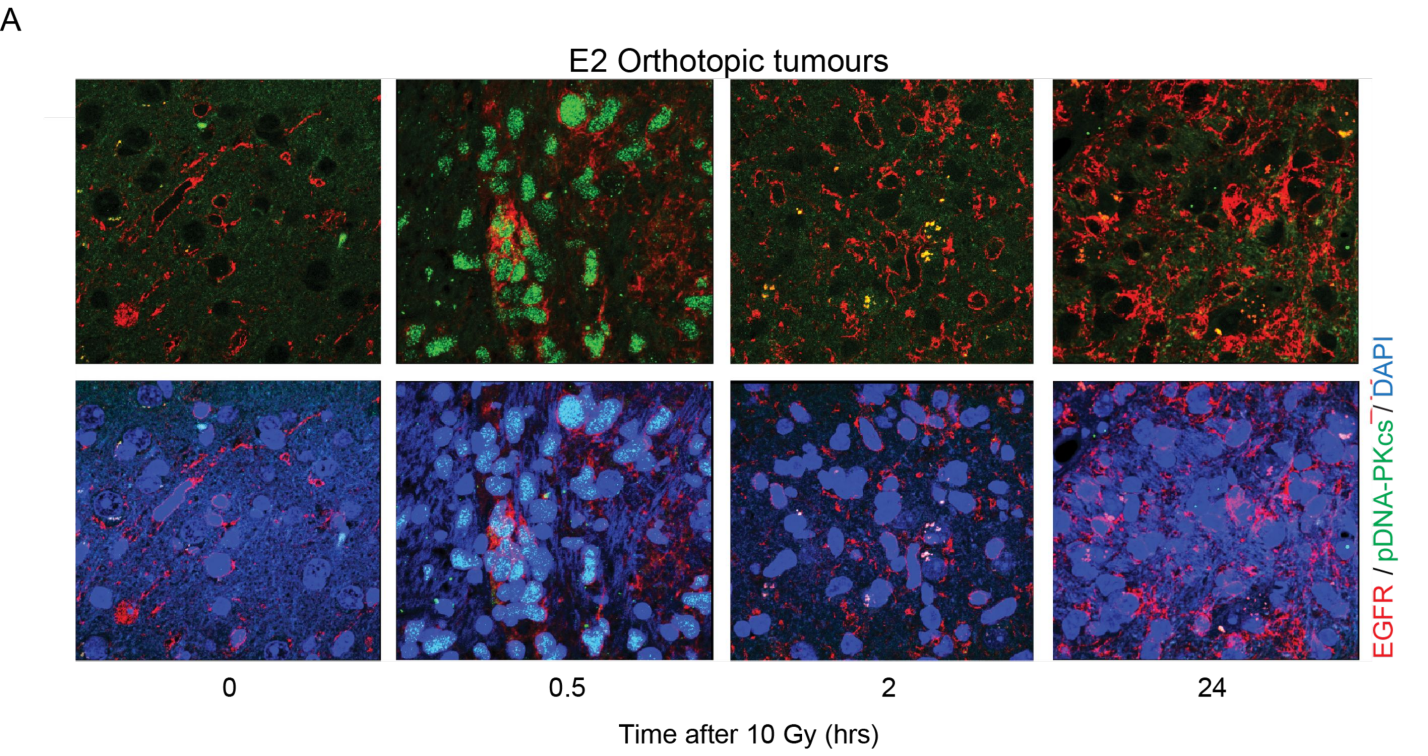

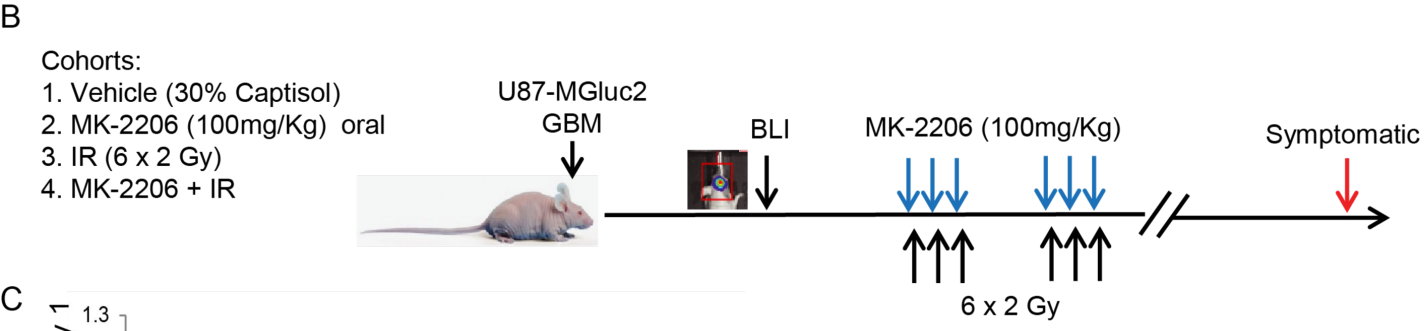

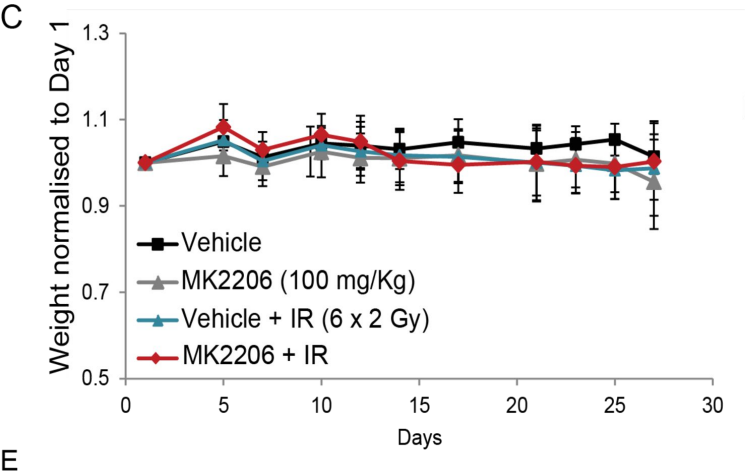

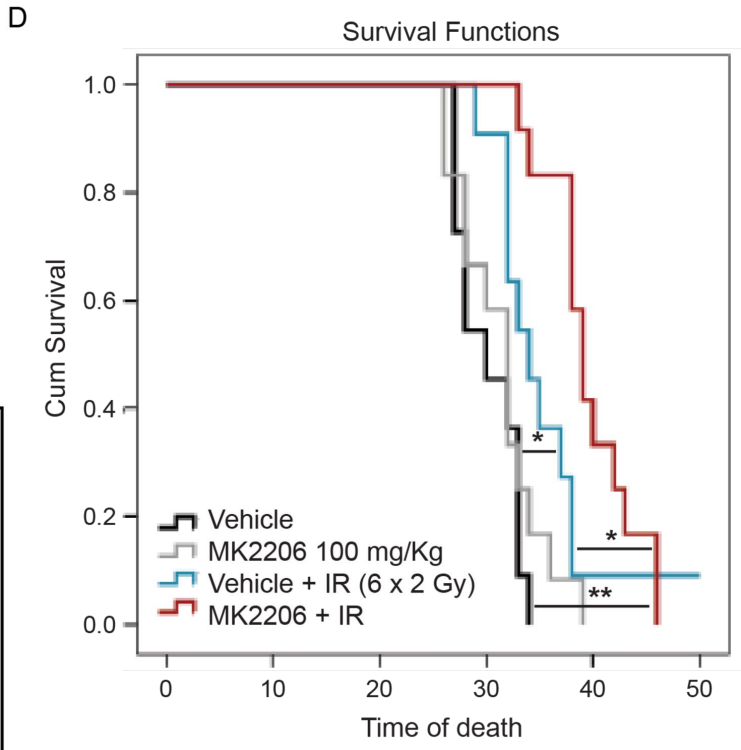

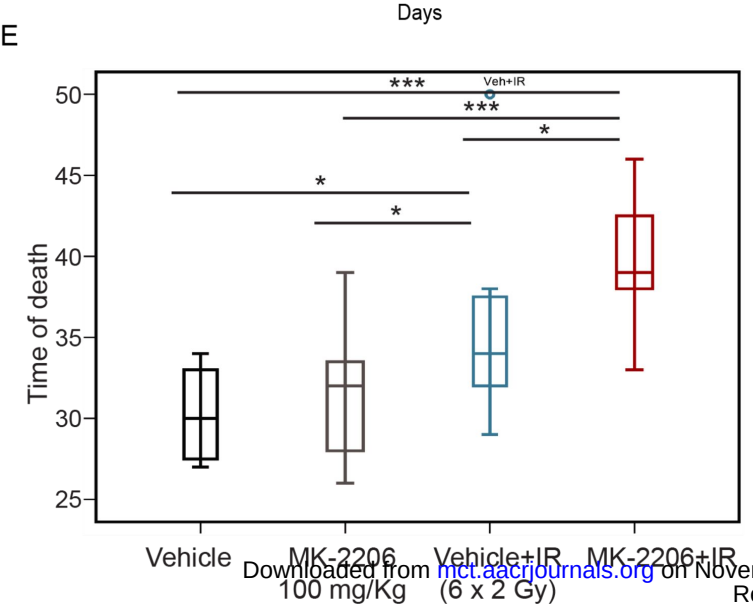

Figure 7

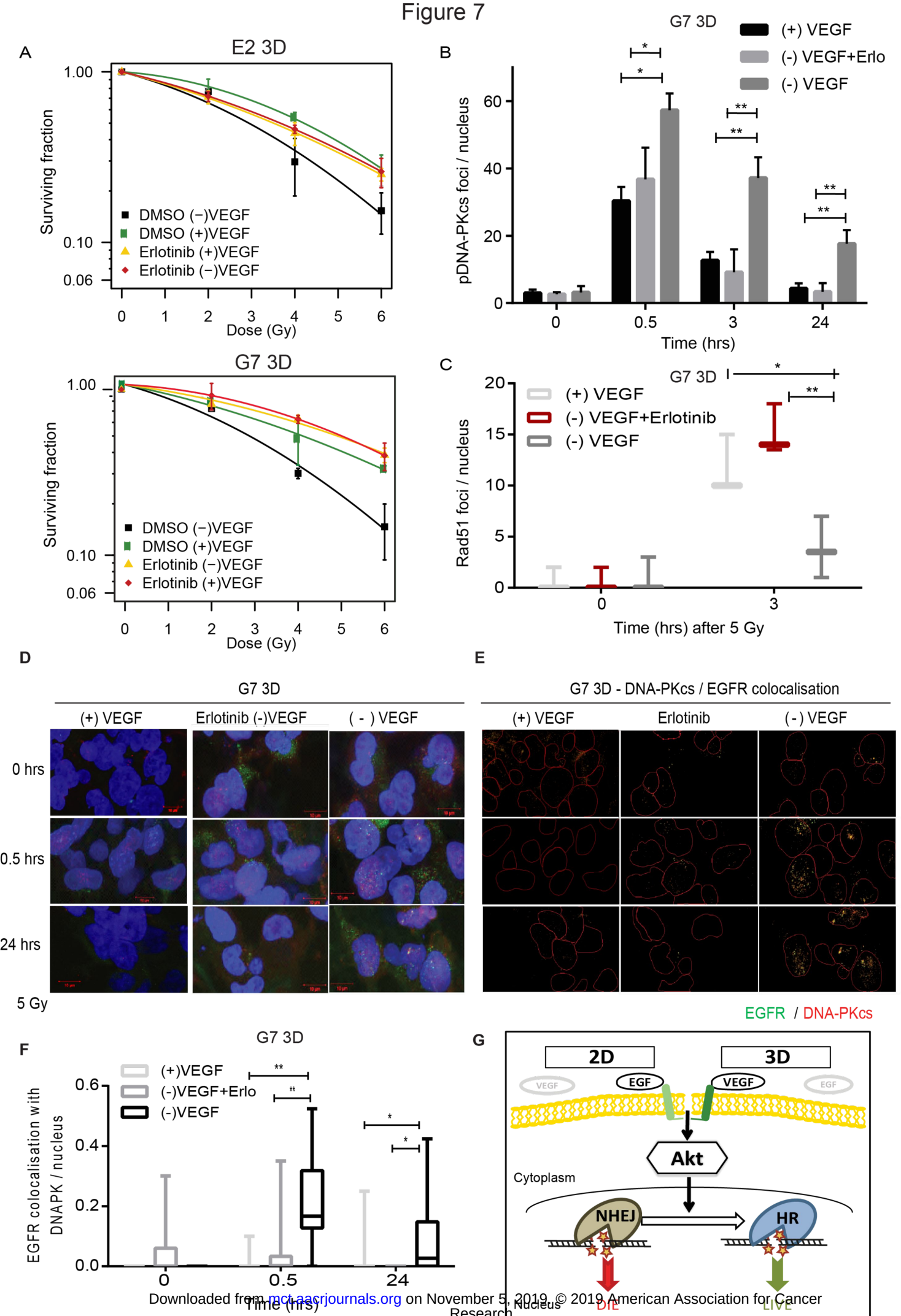

AACR American Association for Cancer Research

Molecular Cancer Therapeutics

Radiation responses of 2D and 3D glioblastoma cells: a novel, 3D-specific radioprotective role of VEGF/Akt signaling through functional activation of NHEJ

Natividad Gomez-Roman, Ming Y Chong, Sandeep K Chahal, et al.

Mol Cancer Ther Published OnlineFirst October 31, 2019.